

Visible light induced hydrogen generation using a hollow photocatalyst with two cocatalysts separated on two surface sides†

Cite this: *Phys. Chem. Chem. Phys.*, 2014, 16, 5937

Received 20th November 2013,
Accepted 9th January 2014

DOI: 10.1039/c3cp54629b

www.rsc.org/pccp

Minh-Hao Pham,^a Cao-Thang Dinh,^a Gia-Thanh Vuong,^a Ngoc-Don Ta^b and Trong-On Do^{*a}

A hollow Fe₂O₃–TiO₂–PtO_x photocatalyst for visible light H₂ generation was prepared from nanosized MIL-88B consisting of coordinatively unsaturated metal centers as a hard template. This photocatalyst is composed of hybrid metal oxide–TiO₂ with controllable wall thickness and two different cocatalysts that are separately located on two surface sides.

Due to the depletion of fossil fuels and the serious environmental problems accompanying their combustion, a new form of energy that is clean, renewable, low-cost and a viable alternative to fossil fuels is urgently needed.¹ Solar-driven H₂ generation using semiconductor photocatalysts represents an attractive pathway towards solving important energy and environmental problems.² However, the significant challenge of using sunlight for H₂ generation lies in designing an efficient system using visible rather than UV light.

To achieve high efficiency, a sunlight-driven photocatalyst is usually composed of a semiconductor that harvests visible light and cocatalysts that are loaded and highly dispersed on the photocatalyst surface to create active sites and reduce the activation energy for gas formation. The cocatalysts are typically a noble metal such as Pt and Rh with reductive sites for H₂ evolution and a metal oxide such as cobalt oxide and manganese oxide with oxidative sites.³ Upon band gap excitation of the photocatalyst, the photogenerated electrons and holes migrate towards the reductive and oxidative surface sites, respectively, thereby facilitating efficient electron–hole separation. This photocatalytic system thus improves the photocatalytic activity, compared to photocatalysts loading only either a reduction or oxidation cocatalyst.⁴ Furthermore, two different cocatalysts, which are highly dispersed and isolated from each other on the

same photocatalyst, are highly desired to promote gas evolution in harmony under visible light irradiation. However, to date, the demonstration of this concept still remains a major challenge.⁵

Among the semiconductor-based photocatalysts (*e.g.*, titanium dioxide,⁶ oxide solid solutions,^{2c,7} and tantalum–nitrogen compounds⁸), TiO₂ is considered to be the most likely candidate for commercial scale-up due to the fact it is inexpensive, nontoxic and a robust photocatalyst under photochemical conditions. Due to its large band gap (3.0 eV and 3.2 eV for rutile and anatase, respectively), TiO₂ only absorbs UV light. Several approaches, including doping with transition metals, such as Fe, Cr, and Cu, non-metals, such as N, S, and C, or hydrogenation, have been taken to narrow the band gap of TiO₂ and thus extend its photoactivity in the visible region.⁹

On the other hand, metal–organic frameworks (MOFs), which are formed by polymeric connections of metal centers, as “clusters”, in coordination with organic linkers, have emerged as an interesting class of materials for diverse applications due to their incredibly tunable properties as well as rationally tailored morphologies.¹⁰ Among them, MOF structures consisting of coordinatively unsaturated metal centers (namely, MOF-UMCs), such as trimeric Cr₃(μ₃-O) or Fe₃(μ₃-O) clusters of MIL-88 and MIL-101, are particularly interesting for this present work. In these types of MOF materials, each trimeric metal(III) center possesses terminal water molecules that can be removed by vacuum and temperature treatments to generate Lewis acid sites. Such dehydrated MOF-UMCs are very beneficial for grafting organic molecules because of their strong interactions with electron-rich functional groups, in which amine functional groups are often used as grafting units.¹¹

Herein, we report a novel route to prepare a new type of photocatalytic hollow metal oxide–TiO₂ nanostructure using nanosized MOF-UMCs as a hard template. This type of hollow nanocomposite is composed of hybrid metal oxide–TiO₂ with controllable wall thickness (15–30 nm) and two distinct functional (*i.e.* oxidative and reductive) cocatalysts that are separately located on the two opposite sides of the hollow: one is made from metal clusters of the MOF framework after calcination, which are

^a Department of Chemical Engineering, Centre en catalyse et chimie verte (C3V), Laval University, Quebec, G1V 0A6, Canada. E-mail: trong-on.do@gch.ulaval.ca
^b School of Chemical Engineering, Hanoi University of Science and Technology, Hanoi, Vietnam

† Electronic supplementary information (ESI) available: Experimental, characterization and additional results. See DOI: 10.1039/c3cp54629b

embedded inside, and the other by metal doping such as PtO_x outside of the hollow. This hollow nanocomposite not only absorbs visible light but also improves the electron-hole separation, due to its thin wall and the isolated location of the two different cocatalysts. As a result, a high visible-light photoactivity is found for H_2 generation.

To illustrate our approach, we selected nanosized MIL-88B which consists of unsaturated $\text{Fe}_3(\mu_3\text{-O})$ clusters as a hard template (noted as MIL-88B-UMCs), due to its dense state and only titanium shell formed on the MIL-88B surface. Titanium(IV)-(triethanolamino)isopropoxide $\text{C}_3\text{H}_7\text{OTi}(\text{OC}_2\text{H}_4)_3\text{N}$ (TEAI), with an amine group as a grafting reagent and H_2PtCl_6 as a Pt source, was used for the synthesis of the hollow $\text{Fe}_2\text{O}_3\text{-TiO}_2\text{-PtO}_x$ nanostructure. Lewis acid sites were generated from MIL-88B-UMCs after the removal of the terminal water molecules by vacuum/temperature treatment to which the amine group of TEAI can be grafted *via* the lone electron pair of the nitrogen atom (Scheme 1). Even though a number of Lewis acid sites were available in the dehydrated framework, TEAI was only grafted on its outer surface. This is due to the dense state of MIL-88B.¹² To increase the shell titania thickness, the TEAI-grafted MIL-88B sample was treated with a dilute solution of TEAI in ethanol with 5 vol% H_2O . During this treatment, the hydrolysis and condensation of TEAI produced a MIL-88B core-TiO₂ shell nanostructure. Furthermore, the thickness of the titania shell can be also controlled by the TEAI concentration.

In a typical procedure, MIL-88B nanocrystals of a desired size were prepared by following the method described in our previous work, using $\text{FeCl}_3 \cdot 6\text{H}_2\text{O}$, 2-amino-1,4-benzenedicarboxylic acid, Pluronic F127 and acetic acid.¹³ The resulting bipyramidal hexagonal prism crystals with an average length and width of ~ 500 nm and ~ 150 nm, respectively, are shown in Fig. 1a and b and Fig. S1a (ESI[†]). The MIL-88B structure with the formula $\text{Fe}_3\text{O}(\text{H}_2\text{N-BDC})_3\text{Cl}(\text{H}_2\text{O})_2$ was also confirmed by powder X-ray diffraction (Fig. S1b, ESI[†]). In the MIL-88B framework, each $\text{Fe}_3(\mu_3\text{-O})$ cluster contains two terminal water molecules. After the removal of these water molecules by dehydration, Lewis acid sites were generated and available for amine grafting.¹⁴ TEM images of the TEAI-grafted MIL-88B sample show no essential change in the morphology of the sample before and after

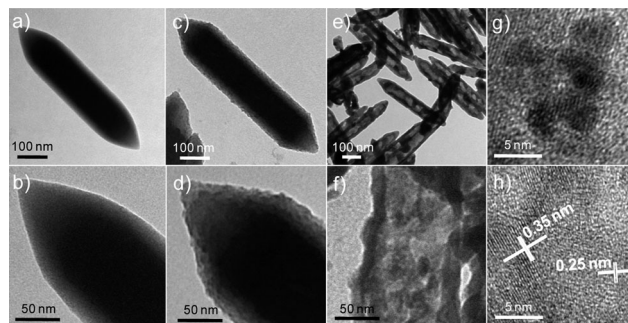
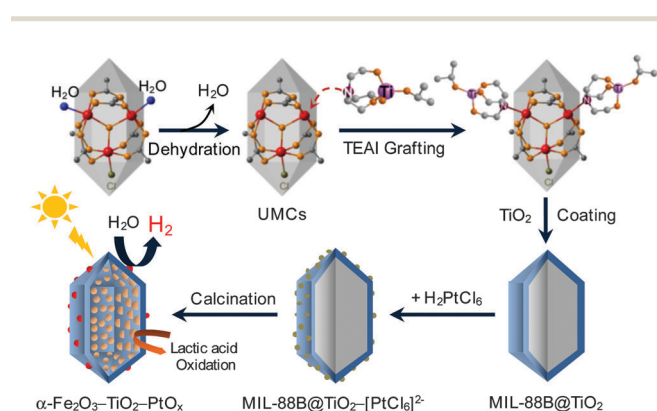


Fig. 1 TEM and HRTEM images of MIL-88B (a and b); MIL-88B@TiO₂ (c and d) and hollow $\text{Fe}_2\text{O}_3\text{-TiO}_2\text{-PtO}_x$ (e-h).

grafting (Fig. S2a and b, ESI[†]). However, the XPS spectrum of the grafted sample exhibits a peak which is characteristic of Ti, indicating that TEAI molecules were grafted on the MIL-88B outer surface (Fig. S2c, ESI[†]). The TEAI-grafted MIL-88B sample was subsequently treated in a refluxing dilute solution of TEAI in ethanol (5 vol% H_2O). The MIL-88B core-TiO₂ shell nanostructure with a controllable titania shell thickness was obtained. TEM images of the as-made MIL-88B core-titania shell nanostructure show almost the same morphology as that of the pristine MIL-88B (Fig. 1c and d and Fig. S3a, ESI[†]). However, this material has a rough surface as compared to the smooth surface of the pristine MIL-88B, indicating the formation of a titania shell on the MIL-88B nanocrystals. The XPS spectra also indicate a large amount of Ti on the sample (Fig. S3b, ESI[†]). The powder XRD pattern of the as-made MIL-88B core-titania shell nanoparticles (*i.e.*, before calcination) exhibits only diffraction peaks which are characteristic of the MIL-88B structure (Fig. 2a); no diffraction peaks characteristic of TiO₂ were observed, indicating the amorphous TiO₂ shell on this sample. This amorphous phase of the TiO₂ shell was also confirmed by the HRTEM observation (Fig. S3a, inset, ESI[†]).

To achieve the hollow photocatalyst with two cocatalysts located on the two opposite sides, the as-made MIL-88B core-titania shell nanomaterial was impregnated with H_2PtCl_6 , followed by calcination in air. After calcination, the color of the sample changed from



Scheme 1 Schematic illustration of the formation of the hollow $\text{Fe}_2\text{O}_3\text{-TiO}_2\text{-PtO}_x$ nanocomposite.

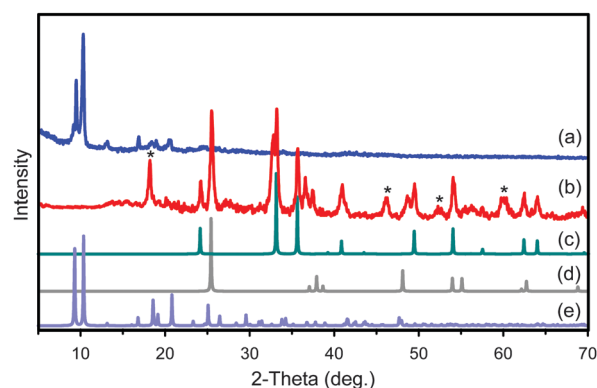


Fig. 2 Powder XRD patterns of MIL-88B@TiO₂ (a) and $\alpha\text{-Fe}_2\text{O}_3\text{-TiO}_2\text{-PtO}_x$ (b); simulated patterns of $\alpha\text{-Fe}_2\text{O}_3$ (c), anatase TiO₂ (d), and MIL-88B (e) for reference.

dark brown to dark red, due to the decomposition of the Fe-based MIL-88B core into iron oxide. Importantly, as shown by TEM (Fig. 1e) and SEM (Fig. S4, ESI[†]) images, no essential change in the morphology of this calcined sample was observed. However, a reduction in size was found.

The TEM image of the calcined sample exhibits clearly a hollow nanostructure with a wall thickness of ~ 15 nm. Note that under the same calcination conditions, the morphology of the pristine MIL-88B nanocrystals (*i.e.*, without titania shell) was destroyed, forming aggregated irregular iron oxide particles (Fig. S5, ESI[†]).

Furthermore, TEM and HRTEM images of the calcined hollow sample show PtO_x nanoparticles with sizes 3–4 nm highly dispersed on the outer side of the hollow surface (Fig. 1f and g). The HRTEM image also indicates that each individual hollow nanoparticle is composed of ultrafine metal oxide particles which are well crystallized with a *d*-spacing of 0.35 nm, matching the *d*₁₀₁ of anatase TiO₂, and 0.25 nm, matching the *d*₁₁₀ of α -Fe₂O₃ (Fig. 1h).

The XRD pattern of the hollow α -Fe₂O₃-TiO₂-PtO_x sample shows diffraction peaks that match those of the anatase TiO₂ and α -Fe₂O₃ phases (Fig. 2b). Four additional peaks (asterisked in Fig. 2b) are characteristic of Fe-titanate mixed oxide (Fe₂TiO₅), which could be formed at the interface of TiO₂ and α -Fe₂O₃. The small peak at 36.6 degrees is an overlap of the peaks of anatase TiO₂ and Fe₂TiO₅.

The formation of the hollow structure and the shrinkage of the MIL-88B core-titania shell structure after calcination are attributed to the decomposition of the MIL-88B core into iron oxide nanoparticles, which occupied much less volume, and the transformation of the amorphous phase to a crystalline phase of the TiO₂ shell under the thermal treatment in air, as demonstrated by thermogravimetric analysis (Fig. S6, ESI[†]). The BET surface area of this hollow α -Fe₂O₃-TiO₂-PtO_x sample is 40 m² g⁻¹. The thickness of the Fe₂O₃-TiO₂ hybrid wall was also controlled by adjusting the concentration of TEAI in the refluxing solution. When the TEAI concentration increases from 6 mM to 50 mM, the thickness increases from 15 nm to 30 nm (Fig. 1f and Fig. S8, ESI[†]). However, at higher concentrations of TEAL, isolated TiO₂ nanoparticles were formed.

XPS was performed to investigate the chemical states of Ti and Fe in the hollow α -Fe₂O₃-TiO₂-PtO_x material (Fig. 3). The Ti 2p spectrum fitted with the Gaussian-Lorentzian function reveals a dominant Ti 2p_{3/2} peak with a binding energy (BE) at

458.0 eV, which is characteristic of a Ti⁴⁺ state in a TiO₂ lattice,¹⁵ along with two shoulders. The first shoulder at 456.5 eV corresponds to a Ti³⁺ state, due to an oxygen deficiency in TiO₂,¹⁶ whilst the second shoulder at 458.6 eV arises from a Ti⁴⁺ state in the Ti-O-Fe structure.¹⁷ In the Ti-O-Fe bond, the Pauling electronegativity differential between Fe³⁺ (1.83) and Ti⁴⁺ (1.54) ions can induce electron transfer from Ti⁴⁺ to Fe³⁺. This makes the Ti⁴⁺ ion less electron rich and Fe³⁺ more electron rich and thus results in an increase of core electron BE of Ti⁴⁺ and a decrease of core electron BE of Fe³⁺. The XPS spectrum of Fe 2p indicates three dominant peaks including Fe 2p_{3/2} at 712.1 eV, Fe 2p_{1/2} at 725.5 eV and a satellite at 719.1 eV, which is consistent with the presence of α -Fe₂O₃.¹⁸ Moreover, the fitted Fe 2p_{3/2} peak shows an additional peak at 710.3 eV, which is assigned to a Fe³⁺ state in the Ti-O-Fe bond. The absence of the Fe 2p_{3/2} peak at 709.3 eV suggests that no Fe²⁺ was present in the sample. The XPS analysis also shows the ratio of Ti and Fe to be 1 : 1.9.

The presence of Ti⁴⁺ and Fe³⁺ states in the Ti-O-Fe bond suggests Fe-doping in the TiO₂ lattice. It is inferred that during calcination, the MIL-88B core is decomposed. In parallel, the amorphous TiO₂ shell is converted to crystalline anatase and some of the iron ions from the MIL-88B enter the TiO₂ lattice, producing Fe-doped TiO₂. Because of a high iron content in MIL-88B@TiO₂, iron oxide nanoparticles are also formed inside the hollow.

The UV-vis diffuse reflectance spectra of the hollow α -Fe₂O₃-TiO₂-PtO_x and TiO₂ (P25) samples are shown in Fig. 4a. The hollow sample absorbs a large visible light region with a band edge around 610 nm. Considering that the absorption edge shifts to the visible light region upon iron doping in TiO₂, the visible light absorption of the hollow hybrid can be attributed to Fe-doped TiO₂, α -Fe₂O₃ and Fe₂TiO₅, in which the absorption of Fe-doped TiO₂ overlaps with that of α -Fe₂O₃ and Fe₂TiO₅. The photocatalytic activity of the hollow α -Fe₂O₃-TiO₂-PtO_x nanocomposite for H₂ generation was carried out under visible light irradiation ($\lambda > 420$ nm) using lactic acid as a sacrificial reagent and 20 mg of the catalyst. The results show that 22 μ mol h⁻¹ of H₂ gas was evolved using this photocatalytic system. To investigate the stability of the α -Fe₂O₃-TiO₂-PtO_x photocatalyst, an experiment of 5 cycles with intermittent N₂ bubbling after every 5 h was also carried out. The results show that no significant change in photocatalytic activity was

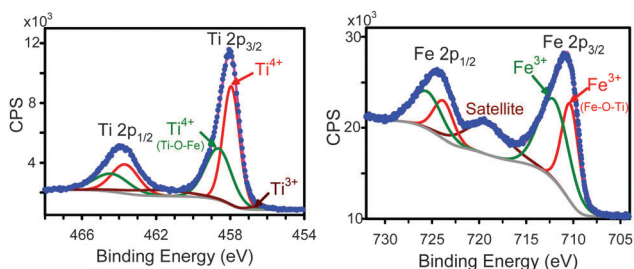


Fig. 3 XPS spectra of Ti 2p and Fe 2p core levels of the hollow α -Fe₂O₃-TiO₂-PtO_x.

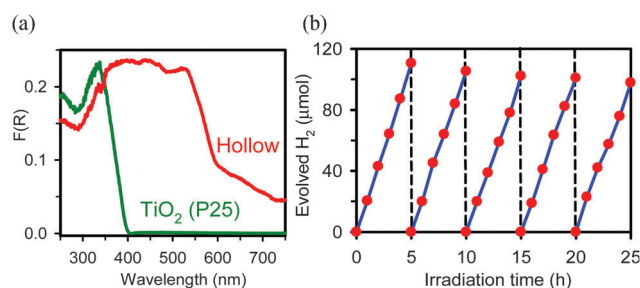


Fig. 4 UV-vis diffuse reflectance spectra of the hollow and TiO₂ (P25) samples (a), and the photoactivity for H₂ generation under visible light irradiation of the hollow Fe₂O₃-TiO₂-PtO_x sample using 20 mg of the catalyst (b).

observed even after 5 cycles (Fig. 4b). The amount of H₂ gas was evolved linearly as a function of time for each cycle, and a total of 110 μmol H₂ was produced after 5 cycles. This indicates a good stability of this type of hollow photocatalysts.

For comparison, a composite of α-Fe₂O₃, TiO₂ and PtO_x with the same chemical composition as the hollow α-Fe₂O₃-TiO₂-PtO_x sample was also prepared using the same synthetic procedure and starting with MIL-88B nanocrystals, except using titanium(IV) butoxide (*i.e.*, without an amine group) as a grafting reagent instead of TEAL. For this calcined sample, only a small quantity of H₂ was produced after 5 h irradiation, under the same photocatalytic conditions. It is obvious that the absence of the amine group in the titanium precursor and the rapid hydrolysis of titanium butoxide in ethanol (5 vol% H₂O) led to a physical mixture of TiO₂ particles and MIL-88B nanocrystals rather than the MIL-88B@TiO₂ core-shell nanostructure (Fig. S9, ESI†). Consequently, no essential H₂ was formed under visible light for this material. Furthermore, when PtO_x-loaded α-Fe₂O₃ powders prepared from MIL-88B, PtO_x-loaded TiO₂ and PtO_x-loaded Fe₂TiO₅ were used under the same photocatalytic conditions, only a trace of H₂ was found in these cases (Table S1, ESI†). In the case of PtO_x-loaded [Fe-doped TiO₂], the same system generated 6 μmol of H₂ gas which is much smaller than the evolved H₂ amount by the α-Fe₂O₃-TiO₂-PtO_x hollow photocatalyst.

Although α-Fe₂O₃ and Fe₂TiO₅ powders absorb visible light, they cannot drive proton reduction because their conduction band (CB) is more positive than the required potential of the 2H⁺/H₂ couple.¹⁹ TiO₂ only absorbs UV light and thus does not catalyze H₂ evolution under visible light. By contrast, Fe-doped TiO₂ with a narrowed band gap resulting from the broadening of the valence band (VB) can absorb visible light and induce proton reduction. Because the VB broadening depends on the level of Fe loading,²⁰ the top of the VB of Fe-doped TiO₂ is located between that of Fe₂O₃ and TiO₂. In the hollow hybrid, the photogenerated holes in the VB of Fe-doped TiO₂ move to Fe₂O₃ nanoparticles for the oxidation of the electron donor and the electrons in the CB of the Fe-doped TiO₂ component migrate to PtO_x nanoparticles for proton reduction into H₂. This generates the separation of photogenerated electron-hole pairs which enhances the photocatalytic activity. Therefore, it is possible that the high photocatalytic activity of the hollow α-Fe₂O₃-TiO₂-PtO_x nanocomposite developed in this work for visible light-driven H₂ generation could be associated with Fe-doped TiO₂, the separation of PtO_x and α-Fe₂O₃ nanoparticles as cocatalysts as well as the thin walls of the hollow (*i.e.*, short migration distance of electrons and holes to the surface). They are key features for an efficient nanocomposite photocatalyst. A further study on this issue is in progress to gain insight into mechanistic aspects of this process.

In conclusion, we have developed an approach towards a new type of hollow hybrid metal-oxide-TiO₂-PtO_x photocatalysts for efficient visible light-driven H₂ generation using nanosized MOFs consisting of coordinatively unsaturated metal centers as the hard template. This approach is expected to extend to other MOF-UMCs, such as HKUST-1 for CuO_x-TiO₂, and MOF-74 isostructural series for MO_x-TiO₂ (M = Co, Mn, Zn).²¹

Notes and references

- (a) M. Gratzel, *Acc. Chem. Res.*, 1981, **14**, 376; (b) N. Armaroli and V. Balzani, *Angew. Chem., Int. Ed.*, 2007, **46**, 52; (c) A. J. Nozik and J. R. Miller, *Chem. Rev.*, 2010, **110**, 6443.
- (a) K. Maeda and K. Domen, *J. Phys. Chem. Lett.*, 2010, **1**, 2655; (b) X. Chen, S. Shen, L. Guo and S. S. Mao, *Chem. Rev.*, 2010, **110**, 6503; (c) K. Ohno, L. Bai, T. Hisatomi, K. Maeda and K. Domen, *J. Am. Chem. Soc.*, 2012, **134**, 8254.
- (a) J. Kiwi, E. Borgarello, E. Pelizzetti, M. Visca and M. Gratzel, *Angew. Chem., Int. Ed.*, 1980, **19**, 646; (b) F. Zhang, A. Yamakata, K. Maeda, Y. Moriya, T. Takata, J. Kubota, K. Teshima, S. Oishi and K. Domen, *J. Am. Chem. Soc.*, 2012, **134**, 8348.
- K. Maeda, A. Xiong, T. Yoshinaga, T. Ikeda, N. Sakamoto, T. Hisatomi, M. Takashima, D. Lu, M. Kanehara, T. Setoyama, T. Teranishi and K. Domen, *Angew. Chem., Int. Ed.*, 2010, **49**, 4096.
- (a) H. Kato, K. Asakura and A. Kudo, *J. Am. Chem. Soc.*, 2003, **125**, 3082; (b) D. Wang, T. Hisatomi, T. Takata, C. Pan, M. Katayama, J. Kubota and K. Domen, *Angew. Chem., Int. Ed.*, 2013, **52**, 1.
- (a) K. Hashimoto, H. Irie and A. Fujishima, *Jpn. J. Appl. Phys.*, 2005, **44**, 8269; (b) A. Kubacka, M. Fernandez-Garcia and G. Colon, *Chem. Rev.*, 2012, **112**, 1555; (c) C. T. Dinh, Y. Seo, T. D. Nguyen, F. Kleitz and T. O. Do, *Angew. Chem., Int. Ed.*, 2012, **51**, 6608.
- (a) K. Maeda, T. Takata, M. Hara, N. Saito, Y. Inoue, H. Kobayashi and K. Domen, *J. Am. Chem. Soc.*, 2005, **127**, 8286; (b) K. Maeda, K. Teramura, D. Lu, T. Takata, N. Saito, Y. Inoue and K. Domen, *Nature*, 2006, **440**, 295.
- (a) G. Hitoki, T. Takata, J. N. Kondo, M. Hara, H. Kobayashi and K. Domen, *Chem. Commun.*, 2002, 1698; (b) M. Higashi, K. Domen and R. Abe, *J. Am. Chem. Soc.*, 2012, **134**, 6968; (c) Y. Li, T. Takata, D. Cha, K. Takanabe, T. Minegishi, J. Kubota and K. Domen, *Adv. Mater.*, 2013, **25**, 125.
- (a) R. Asahi, T. Morikawa, T. Ohwaki, K. Aoki and Y. Taga, *Science*, 2001, **293**, 269; (b) S. U. M. Khan, M. A. Shahry and W. B. Ingler Jr., *Science*, 2002, **297**, 2243; (c) X. Chen and S. S. Mao, *Chem. Rev.*, 2007, **107**, 2891; (d) X. Chen, L. Liu, P. Y. Yu and S. S. Mao, *Science*, 2011, **331**, 746.
- (a) H. C. Zhou, J. R. Long and O. M. Yaghi, *Chem. Rev.*, 2012, **112**, 673; (b) G. Ferey, *Chem. Soc. Rev.*, 2008, **37**, 191; (c) A. Umemura, S. Diring, S. Furukawa, H. Uehara, T. Tsuruoka and S. Kitagawa, *J. Am. Chem. Soc.*, 2011, **133**, 15506; (d) M. H. Pham, G. T. Vuong, F. G. Fontaine and T. O. Do, *Cryst. Growth Des.*, 2012, **12**, 3091.
- (a) Y. K. Hwang, D. Y. Hong, J. S. Chang, S. H. Jhung, Y. K. Seo, J. Kim, A. Vimont, M. Daturi, C. Serre and G. Ferey, *Angew. Chem., Int. Ed.*, 2008, **47**, 4144; (b) M. Banerjee, S. Das, M. Yoon, H. J. Choi, M. H. Hyun, S. M. Park, G. Seo and K. Kim, *J. Am. Chem. Soc.*, 2009, **131**, 7524.
- G. T. Vuong, M. H. Pham and T. O. Do, *Dalton Trans.*, 2013, **42**, 550.

- 13 M. H. Pham, G. T. Vuong, A. T. Vu and T. O. Do, *Langmuir*, 2011, **27**, 15261.
- 14 S. Surble, C. Serre, C. M. Draznieks, F. Millange and G. Ferey, *Chem. Commun.*, 2006, 284.
- 15 B. M. Reddy, B. Chowdhury and P. G. Smirniotis, *Appl. Catal., A*, 2001, **219**, 53.
- 16 J. P. Espinos, A. Fernandez and A. R. Gonzalez-Elipe, *Surf. Sci.*, 1993, **295**, 402.
- 17 (a) L. Pan, J. J. Zou, X. Zhang and L. Wang, *Ind. Eng. Chem. Res.*, 2010, **49**, 8526; (b) E. Wang, W. Yang and Y. Cao, *J. Phys. Chem. C*, 2009, **113**, 20912.
- 18 T. Yamashita and P. Hayes, *Appl. Surf. Sci.*, 2008, **254**, 2441.
- 19 Y. Matsumoto, *J. Solid State Chem.*, 1996, **126**, 227.
- 20 S. George, S. Pokhrel, Z. Ji, B. L. Henderson, T. Xia, L. Li, J. I. Zink, A. E. Nel and L. Madler, *J. Am. Chem. Soc.*, 2011, **133**, 11270.
- 21 (a) S. S.-Y. Chui, S. M.-F. Lo, J. P. H. Charmant, A. G. Orpen and I. D. Williams, *Science*, 1999, **283**, 1148; (b) N. L. Rosi, J. Kim, M. Eddaoudi, B. Chen, M. O'Keeffe and O. M. Yaghi, *J. Am. Chem. Soc.*, 2005, **127**, 1504; (c) W. Zhou, H. Wu and T. Yildirim, *J. Am. Chem. Soc.*, 2008, **130**, 15268.

Visible Light Induced Hydrogen Generation using a Hollow Photocatalyst with Two Cocatalysts Separated on Two Surface Sides

Minh-Hao Pham,^a Cao-Thang Dinh,^a Gia-Thanh Vuong,^a Ngoc-Don Ta,^b and Trong-On Do^{a,}*

^a Department of Chemical Engineering, Centre en catalyse et chimie verte (C₃V), Laval University, Quebec, G1V 0A6, Canada

^b School of Chemical Engineering, Hanoi University of Science and Technology, Hanoi, Vietnam

Corresponding Author: trong-on.do@gch.ulaval.ca

SUPPORTING INFORMATION

Chemicals

FeCl₃·6H₂O (Aldrich, 97 %), Fe(NO₃)₃·9H₂O (Aldrich, ≥ 98 %), 2-amino-1,4-benzenedicarboxylic acid (Aldrich, 99 %), Pluronic F127 (EO₉₇PO₆₉EO₉₇, average M_n = 12,600, Aldrich), CH₃COOH (Fisher, 99.7 %), titanium(IV) (triethanolaminate)isopropoxide (80 wt% in 2-propanol, Aldrich), titanium(IV) butoxide (Aldrich, 97 %), 2-propanol (Aldrich, 99.5 %), titanium(IV) tetraisopropoxide (Aldrich, 97 %), ethanol (95 %), H₂PtCl₆·6H₂O (Aldrich, ≥ 37.5 % Pt basis) and lactic acid (Aldrich, 85–90 % in water). All chemicals were used as received without further purification.

Synthesis of MIL-88B nanocrystals

MIL-88B nanocrystals were prepared by following our previously reported approach.¹³ Briefly, the aqueous dispersion (15 mL) of 2-aminoterephthalic acid (60 mg, 0.33 mmol), FeCl₃·6H₂O (180 mg, 0.66 mmol), Pluronic F127 (160 mg) and acetic acid (0.6 mL, 10.5 mmol) was heated at 110 °C for 24 h. The resulting solid was isolated and washed several times with ethanol by centrifugation to remove the surfactant and excess reactants.

Titanium precursor grafting on MIL-88B nanocrystals

The as-made MIL-88B (100 mg) was dried overnight at 150 °C under vacuum to remove terminal water molecules. To this dehydrated form, 2 M TEAI solution in 2-propanol (4 mL) was poured and stirred at room temperature for 2 h. The TEAI-grafted MIL-88B was then collected, washed with 2-propanol by centrifugation and dried overnight at 100 °C.

TiO₂ coating on MIL-88B nanocrystals

TEAI-grafted MIL-88B (100 mg) was dispersed in 80 mL of 6 mM TEAI solution in ethanol (5 vol. % H₂O) and then refluxed for 24 h under vigorous stirring. The MIL-88B@TiO₂ core-shell was collected and washed several times with ethanol by centrifugation.

Preparation of α-Fe₂O₃-TiO₂-PtO_x

0.57 mL of H₂PtCl₆ aqueous solution (10 mM) was added to the suspension of MIL-88B@TiO₂ (100 mg) in deionized water (12 mL) and stirred for 1 h at room temperature, followed by a rotary evaporation with a water bath at 50 °C to remove the water. The resulting product was calcined in air with heating rate at 5 °C min⁻¹ at 500 °C for 3 h to yield a dark red PtO_x-loaded composite.

Preparation of PtO_x-[Fe-doped TiO₂]

Fe-doped TiO₂ (Fe/Ti = 0.01) was prepared by sol-gel method.^{S1} 50 mL of ethanol solution containing 5 mL of titanium(IV) tetraisopropoxide was added dropwise into 50 mL of distilled water containing

45 mg of $\text{FeCl}_3 \cdot 6\text{H}_2\text{O}$ (pH adjusted to 1.5 with nitric acid) under vigorous stirring. After stirred for 24 h, the resulted solution was evaporated at 45 °C using a rotary evaporator and dried at 70 °C overnight. The obtained powder was calcined at 400 °C for 1 h to obtain Fe-doped TiO_2 . The loading of PtO_x cocatalyst on the Fe-doped TiO_2 was the same as the procedure for $\alpha\text{-Fe}_2\text{O}_3\text{-TiO}_2\text{-PtO}_x$.

Preparation of $\text{PtO}_x\text{-[Fe}_2\text{TiO}_5]$

Fe_2TiO_5 (Fe/Ti = 1) was prepared by sol-gel method.^{S2} 50 ml of 2-propanol solution containing 3.5 g of $\text{Fe}(\text{NO}_3)_3 \cdot 9\text{H}_2\text{O}$ was added into 20 mL of 2-propanol solution containing 3.0 mL of titanium(IV) butoxide, followed by dropwise addition of 0.7 mL H_2O under stirring. After stirred for 4 h and further aged for 12 h, the mixture was evaporated at 70 °C and dried at 120 °C for 4 h. The obtained powder was calcined at 350 °C for 1 h and 700 °C for 5 h to obtain Fe_2TiO_5 . The loading of PtO_x on the Fe_2TiO_5 was the same as the procedure for $\text{PtO}_x\text{-[Fe-doped TiO}_2]$.

Photocatalytic H_2 evolution

Visible light-induced H_2 evolution was carried out in 300 mL septum-sealed glass reactor. In each run, 20 mg of the photocatalyst was well dispersed with magnetic stirring in a 50 mL of aqueous solution containing lactic acid (10 wt.%). The reactor was deoxygenated by bubbling nitrogen to remove oxygen and then placed in front of a 300 W Xe-lamp with a 420 nm cut-off filter (FSQ-GG420, Newport) under constant stirring. 0.5 mL of the gas in the headspace of the reactor was analyzed by GC to determine the amount of evolved H_2 .

Characterizations

Transmission electron microscopy (TEM) images were obtained on a JEOL JEM 1230 microscope operating at 120 kV. High resolution TEM images were performed on a Tecnai G² 20 instrument operated at 200 kV. Scanning electron microscopy (SEM) images were taken on a JEOL 6360 instrument at an accelerating voltage of 3 kV. Powder X-ray diffraction (XRD) patterns were collected on a Bruker SMART APEX II X-ray diffractometer with $\text{Cu K}\alpha$ radiation ($\lambda = 1.5406 \text{ \AA}$) at a scan rate of $1.0^\circ \text{ min}^{-1}$. All samples were dried at 100 °C overnight to remove guest solvent molecules within the pores before the XRD scan. XPS measurements were carried out in an ion-pumped chamber (evacuated to 10^{-9} Torr) of a photoelectron spectrometer (Kratos Axis-Ultra) equipped with a focused X-ray source ($\text{Al K}\alpha$, $h\nu = 1486.6 \text{ eV}$). The UV-vis spectra were recorded on a Cary 300 Bio UV-visible spectrophotometer. N_2 adsorption-desorption isotherms were carried out at the temperature of liquid nitrogen with a Quantachrome Autosorb-1 system. The BET surface areas were calculated in the range of 0.05–0.3 P/P₀. Thermogravimetric analysis (TGA) was performed with a TGA/SDTA 851e

thermogravimetric analyzer from room temperature to 600 °C with a heating rate of 5 °C min⁻¹ under an air flow of 50 mL min⁻¹.

Operation conditions for GC analysis:

- + Carrier gas: nitrogen at 15 Psi
- + Column: Carboxen-1010 Plot Capillary 30 m x 0.53 mm.
- + Detector: TCD
- + Column temperature: 30 °C
- + Retention time of H₂: 0.9 min

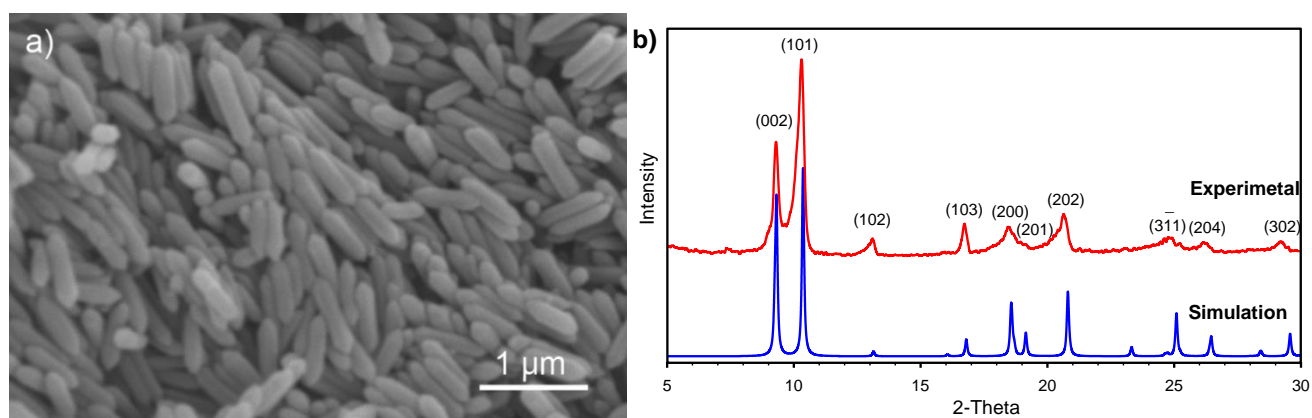


Fig. S1 SEM image (a) and XRD pattern (b) of the starting MIL-88B nanocrystals

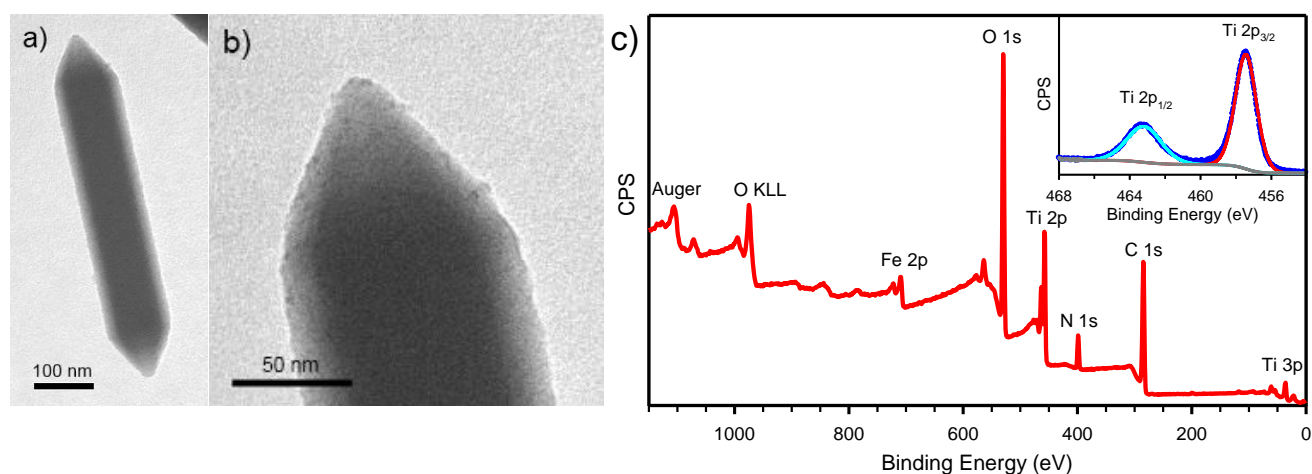


Fig. S2 TEM images (a, b), XPS survey and high-resolution Ti 2p (inset) spectra (c) of TEAI-grafted MIL-88B nanocrystals.

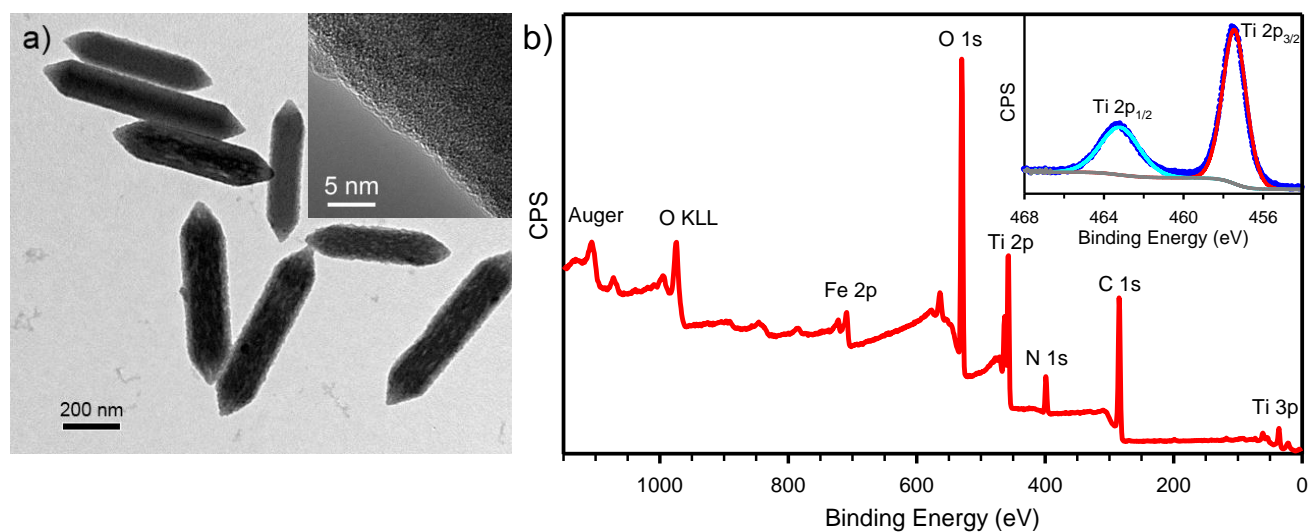


Fig. S3 TEM and HRTEM (inset) images (a), XPS survey and high-resolution Ti 2p (inset) spectra (b) of coated MIL-88B@TiO₂ nanoparticles prepared with the concentration of TEAI at 6 mM TEAI.

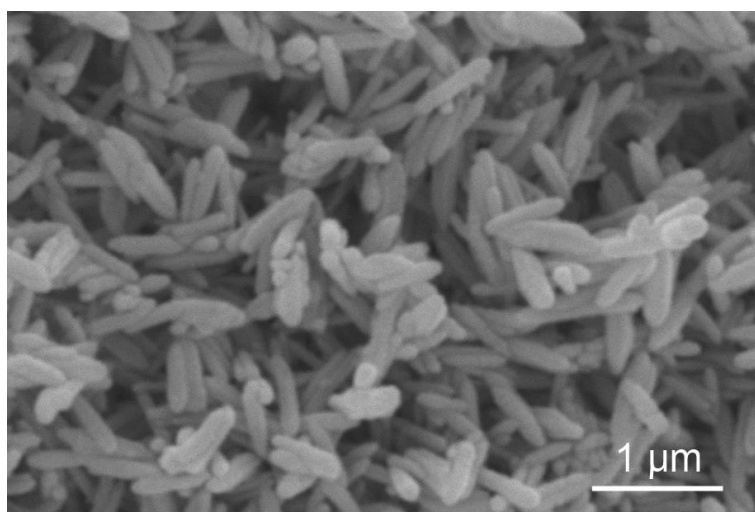


Fig. S4 SEM image of the $\alpha\text{-Fe}_2\text{O}_3\text{-TiO}_2\text{-PtO}_x$ sample after calcination.

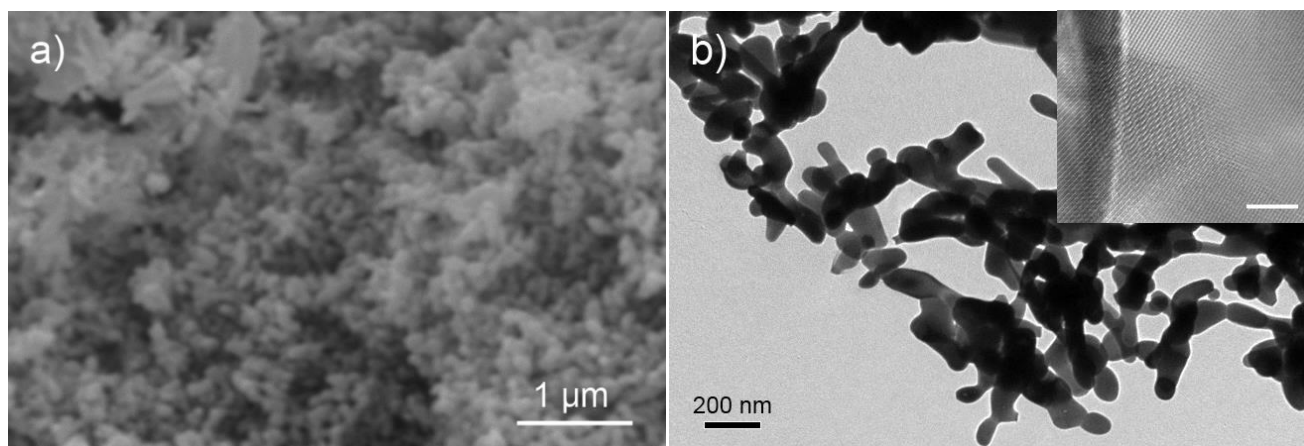


Fig. S5 SEM (a) and TEM (b) images of the iron oxide sample obtained after calcination of the pristine MIL-88B nanocrystals. HRTEM image (inset) indicates the fusion of iron oxide nanoparticles. (scale bar of 5 nm).

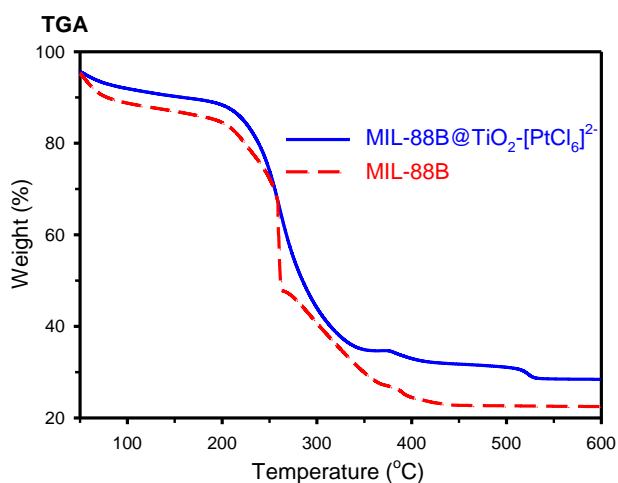


Fig. S6 Thermogravimetric analysis (TGA) of MIL-88B and MIL-88B@TiO₂-[PtCl₆]²⁻. The weight retention differential of 8.0 % at 500 °C attributed to the coated TiO₂ and loaded PtO_x.

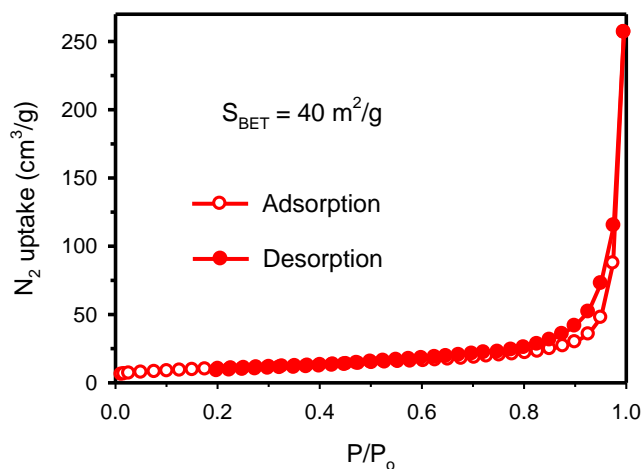


Fig. S7 N₂ adsorption-desorption isotherms at 77 K of the α -Fe₂O₃-TiO₂-PtO_x sample

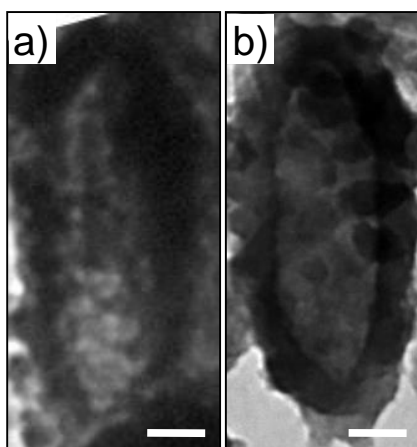


Fig. S8 The hollow nanoparticles with various thicknesses of Fe₂O₃-TiO₂ hybrid wall prepared with the concentration of TEAI at 25 mM (a) and 50 mM (b) while keeping the same other reaction parameters (scale bar of 50 nm).

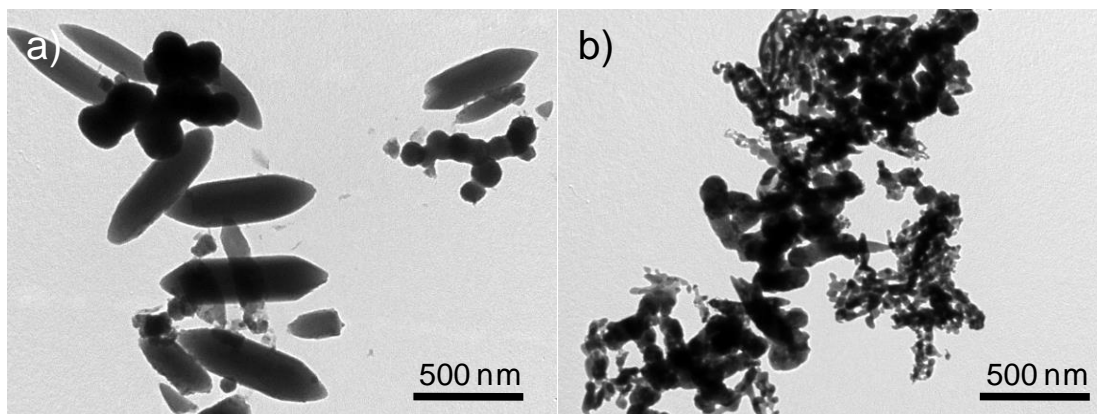


Fig. S9 TEM images of the sample prepared using titanium (IV) butoxide without amine group as grafting reagent instead of TEAI: A separated mixture of TiO₂ nanoparticles and MIL-88B nanocrystals before calcination (a), and TiO₂ particles and Fe₂O₃ particles after calcination (b).

Table S1 Photocatalytic activities of the hollow hybrid and the benchmarks for H₂ evolution

Photocatalyst	Precursor	Evolved H ₂ gas ($\mu\text{mol}\cdot\text{h}^{-1}$)
Fe ₂ O ₃ -TiO ₂ -PtO _x Hybrid	TEAI	22
Fe ₂ O ₃ -TiO ₂ -PtO _x Mixed Oxide	Ti(OBu) ₄	trace
PtO _x -Fe ₂ O ₃	Pristine MIL-88B	trace
PtO _x -TiO ₂	P25	trace
PtO _x -Fe ₂ TiO ₅	Fe/Ti = 1.0 ^(S2)	trace
PtO _x -[Fe-doped TiO ₂]	Fe/Ti = 0.01 ^(S1)	6
Without catalyst	–	0

References

- S1 J. Choi, H. Park, M. R. Hoffmann, *J. Phys. Chem. C* 2010, **114**, 783.
- S2 A. Khaleel, *Colloids and Surfaces A: Physicochem. Eng. Aspects* 2009, **346**, 130.